JOURNAL OF MATERIALS SCIENCE 24 (1989) 2765–2774

# Effect of short-time thermal oxidation on the surface of Al–Li–Cu–Mg alloy (8090) sheet

P. G. PARTRIDGE, NICOLA C. CHADBOURNE*
*Materials and Structures Department, Royal Aerospace Establishment, Farnborough, Hampshire, UK*

The oxidation behaviour of 8090 Al–Li alloy sheet was studied after exposure for short times (< 5 min) in laboratory air, moist air, moist argon and hydrogen at 530° C. Oxidation was greater at grain boundaries in hydrogen but not in air. Sites of rapid local oxidation (number density 9 to 8 × $10^3$ $cm^{-2}$) were associated with insoluble particles. Four types of growth morphology were identified with these sites. Some growths believed to be spinel, were 10 to 25 $\mu$m diameter and grew to ~ 1 mm in height at 2 $\mu m\,sec^{-1}$. Pits beneath these growths were ~ 25 $\mu$m diameter and 10 to 20 $\mu$m deep. A qualitative model is proposed for rapid oxidation in Al–Li alloys and the effect of these sites on weight gain measurements, surface contamination and mechanical properties is discussed.

## 1. Introduction

The addition of lithium to aluminium alloys can increase the elevated temperature oxidation rates by one or two orders of magnitude [1–4]. This is a consequence of the high diffusivity and reactivity of lithium and of the non-protective nature of the lithium-containing oxidation products on the surface of Al–Li alloys. A summary of the oxidation studies reported for binary and ternary Al–Li alloys is given in Table I. These have included exposure to vacuum and various gaseous environments (e.g. air, Ar, $H_2$, $N_2$ and $CO_2$/$N_2$ and $O_2$/Ar mixtures) in dry and moist conditions at temperatures up to 575° C and for times up to 16 h. Weight-gain data and X-ray and electron-beam analytical techniques have been used to relate the surface oxidation products to the oxidation conditions. Oxidation was found to be sensitive to moisture which could lead to a further factor of ten increase in the weight gain [1–3] and to an increase in the hydrogen content of the alloy [2, 3, 13].

Lithium oxidizes preferentially at the free surface of Al–Li alloys and many oxidation reactions are thermodynamically favoured [2]. The following Reactions 1 to 4 are in order of decreasing $\Delta G$, the free energy change, and lead to the products most frequently detected on Al–Li alloy surfaces

$$4Li + O_2 \rightarrow 2Li_2O \quad (1)$$

$$2.5\ Li + 0.5\ Al + H_2O \rightarrow 0.5\ LiAlO_2 + 2\ LiH \quad (2)$$

$$2\ Li + H_2O \rightarrow Li_2O + H_2 \quad (3)$$

$$Li_2O + CO_2 \rightarrow Li_2CO_3 \quad (4)$$

The mass and volume changes that occur when lithium metal is converted to these solid oxidation products are given in Table II. A substantial increase in weight occurs in all the examples with the greatest increase for the $Li_2CO_3$ phase.

Oxidation studies on 8090 alloy at 500° C suggested [10] that $Li_2O$ occurred in dry air (Reaction 3) and $LiAlO_5$ in moist air. The $Li_2O$ phase tends to react in air at room temperature to form LiOH and $Li_2CO_3$ (Reaction 4). After oxidation of 8090 alloy in laboratory air at 530° C for times less than 5 min, lithium and magnesium oxides were detected [12]. The oxide $\alpha Li_5AlO_4$ increased with time and $Li_2CO_3$ was observed after 5 min; after 60 min $\gamma LiAlO_2$ (Reaction 2) was detected. The most common phases on 2090 alloy oxidized at 550° C in dry and moist air were $\gamma LiAlO_2$, $\beta LiAlO_2$ and $Li_2CO_3$. The latter phase tends to become dominant on these alloys after long exposure times in air [12]. The incorporation of lithium into the $Al_2O_3$ film is known [1] to dramatically reduce the resistance to oxidation, and the initial parabolic weight gain curve associated with the formation of oxides and spinels changes to a linear weight gain curve as the $Li_2CO_3$ phase increases [2]. The carbonate film is usually cracked and a number of workers have noted that $Li_2O$, LiH and $Li_2CO_3$ films were removed by washing in water [2, 12, 13] whilst the spinels were unaffected.

Volume changes and thermal stresses cause cracking of surface films and the surface area may be increased by porosity associated with hydrogen [2, 11, 13] or Kirkendall diffusion [11]. These factors and the occurrence of all the oxidation products together in surface films, preclude the use of gravimetric data for determining oxidation rates for Al–Li alloys [1, 2, 10], nor can the depth of the lithium-depleted layer be used to predict oxide layer thickness as suggested elsewhere [14]. Furthermore the use of X-ray diffraction data to relate the amount of each oxidation product to the oxidation conditions is made difficult by the lack of sensitivity at low volume fractions [12], by the variety of oxidation products, by the

* *Present address*: Aeronautical and Mechanical Engineering Department, University of Salford, UK.

0022–2461/89 $03.00 + .12  

TABLE I Summary of oxidation studies on Al–Li alloys

| Alloy composition (wt %) | Test piece dimensions | Surface conditions | Atmosphere | Temperature (°C) | Time | Data or technique* | Reference |
|---|---|---|---|---|---|---|---|
| Al–Mg–Li<br>Al–2 Li | 1.6–2 mm thick sheet | – | Air<br>Salt bath | 450–550 | 1–100 h | XD<br>ED<br>$H_2$ content<br>Hardness | [5] |
| Al–3 Li<br>Al–4.2 Li<br>Al–3 Li–2 Mg | 0.2 mm thick sheet | Electropolished + 14 d in air | 20% $O_2$/Ar dry and wet | 480–575 | 30 min–5 h | Weight gain<br>TEM<br>ED<br>SEM | [3] |
| Al–Zn–Mg + 0.19 Li | 0.5 mm thick sheet | Electropolished | Vacuum, air | 350–500 | $\frac{1}{2}$–1 h | Weight gain<br>TEM | [6] |
| Al–Zn–Mg + Cr, Cu or Li trace additions | 0.5 mm thick sheet | Electropolished | Vacuum, air | 400–500 | 0.5–4 h | X-ray<br>SIMS<br>AES | [7] |
| Al + trace additions | Foil | Pre-oxidized at 240–400° C 2–16 h | 90% r.h. air | 40 | 0–16 d | X-ray<br>SEM<br>EPMA<br>SIMS | [8] |
| Al–Li alloys + trace additions | 0.2 mm thick sheet | Electropolished + 14 d in air | 20% $O_2$/Ar<br>Lab. air<br>$N_2$<br>wet and dry | 350–575 | 30 min–5 h | Weight gain<br>SEM | [4] |
| 8090† | 3 and 5 mm thick sheet | Ground polished pickled anodized | Dry argon air | 480–575 | 20 min–4 h | Hardness<br>EDS (Mg loss)<br>Fatigue<br>Tensile<br>Metallography fractography | [9] |
| Al–Li<br>Al–Li–Zr<br>Al–Li–Cu–Zr<br>8090/8091† | 0.38 mm thick sheet | Electropolished + 4 w in air | Dry or wet air dry, argon | 500 | 1 h, 3 h | Weight gain tensile, bend hardness | [1] |
| 8090†<br>8091† | 7 and 7.8 mm sheet | Electropolished + 1 d in air | Air wet and dry, argon | 500 | 1, 4, 16 h | Li probe weight gain metallography | [10] |
| 2090† | 1 mm thick sheet | Ground | Air, and $CO_2/N_2$, dry and moist, dry $N_2$ | 200–550 | 0–16.6 h | Weight gain<br>XD<br>$H_2$ content<br>SEM | [2] |
| 8090†<br>8091†<br>2090†<br>Al–Li | 7 mm thick plate<br>7.8 mm thick plate<br>12.5 mm plate<br>extrusion 6.25 × 37 mm | As-received<br>Ground<br>Electropolished<br>Sand Blasted<br>Rolled | Vacuum<br>$H_2$<br>Argon<br>Dry and moist air | 500 | 1–6 h | Metallography | [11] |
| 8090† | Extruded bar, 1–3 mm thick test pieces | Etched | Air | 530 | 2.5 min–1 h | Hardness<br>EDS (Mg loss)<br>AES<br>XPS<br>SEM<br>XD* | [12] |
| Al–3 Li<br>2090† | 1/4 in. plate machined to 3 mm diameter | Electropolished | Air, dry and moist<br>$H_2$ | 550 | 12 h | SEM<br>fractography | [13] |

† 8090, Al–2.5 Li–1.4 Cu–0.65 Mg–0.14 Zr, 8091, Al–2.47 Li–2.0 Cu–0.58 Mg–0.12 Zr, 2090, Al–2.7 Cu–1.9 Li–0.16 Zr (wt %).
* XD = X-ray diffraction, ED = electron diffraction, TEM = transmission electron microscopy, SEM = scanning electron microscopy, EDS = energy dispersive X-ray analysis, AES = Auger electron spectroscopy, XPS = X-ray photo-electron-spectroscopy, SIMS = secondary ion mass spectrometry.

large changes in oxide thickness over small distances on the alloy surface [2] and by subsequent reactions of the oxidation products in air at room temperature [2].

Much of the published work referred to above involved long exposure times and thick surface films. In practice, heat-treatment times for thin sheet are kept to a minimum to reduce lithium depletion of the surface [9, 15–17] and to avoid contamination of surfaces prior to solid state diffusion bonding. To clarify the oxidation behaviour during short-time

TABLE II Mass and volume ratios for lithium oxidation [2]

| Oxidation product | Product mass / Metal mass | Product volume / Metal volume |
|---|---|---|
| $Li_2O$ | 2.10 | 0.57 |
| $LiAlO_2$ | 1.94 | 1.12 |
| $Li_2CO_3$ | 5.32 | 1.35 |

oxidation some experiments were carried out on 8090 Al–Li alloy sheet. The results obtained are described in this paper.

## 2. Experimental technique

Sheet with the 8090 alloy composition given in Table I was supplied in the recrystallized and unrecrystallized states. Oxidation specimens 15 mm × 10 mm × 2.5 mm were mechanically polished to 1 $\mu$m diamond finish to remove the lithium-depleted layer. Some species were then electropolished in a 4:1 ethanol and perchloric acid bath for 2 min. Oxidation was carried out in a tube furnace with a hot zone at 560° C. Specimens were attached to a sheathed thermocouple and held by aluminium foil at the edges. Argon or air passed through distilled water at 21° C, or laboratory air or hydrogen from a cylinder was passed through the tube at $\sim 200\,cm^3\,min^{-1}$. The specimen was placed in the cold zone until the atmosphere was stabilized and then inserted into the hot zone. As the temperature approached 520° C the specimen was removed progressively to a cooler part of the tube until 500 to 530° C ± 2° C was reached in ~3 min heating-up time. Specimens were either removed immediately or held for various times up to 1 h before removing to the cold zone to cool to 50° C and then transferring to a scanning electron microscope within 10 min. Some specimens were washed for 5 min in running water and cleaned for 2 min in an ultrasonic bath containing water or acetone to remove surface coatings.

## 3. Results

### 3.1. Surface oxidation at grain boundaries and grain interiors

In a direction normal to the sheet surface prior to oxidation, the grain width was 2 to 6 $\mu$m and no lithium-depleted layer was visible (Fig. 1). After an anneal in moist argon or laboratory air at 530° C, a continuous film was present on the grain interiors at A but not at the grain boundaries at B in Figs 2 and 3 for unrecrystallized and recrystallized sheet, respectively.

An anneal for 2 min in a hydrogen atmosphere produced a thick grain-boundary film at A in Fig. 4a and a fine-scale nodular film on the grain interior. These films were removed by washing for 5 min in flowing water. It was concluded that the air film was characteristic of $Li_2CO_3$ [2] and the film produced in hydrogen was probably LiH [13]. After washing, the carbonate-free surface appeared similar to the unoxidized surface but the hydride-free surface showed grain-boundary grooves and pits in the grain interior (Fig. 4b). The carbonate film was cracked and sometimes flaked off during cooling from the oxidation temperature.

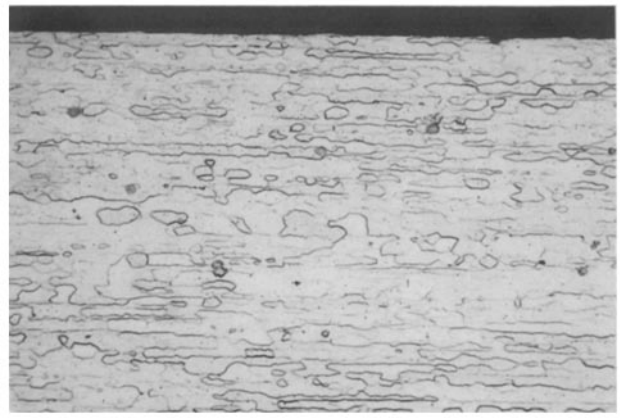

*Figure 1* Section through unrecrystallized sheet prior to oxidation, ×375.

### 3.2. Rapid oxidation sites

Some specimens held at 530° C in air or argon for times less than 1 min showed little continuous film formation but did show evidence of rapid local oxidation at isolated sites. At these rapid oxidation sites, four types of growth morphology were identified. The most common (Type 1) occurred as roughly hemispherical or slightly conical mounds up to 25 $\mu$m diameter and 25 $\mu$m in height as shown at C in Figs 3a and b. These growths were often layered normal to the growth direction and penetrated pre-existing films; growth appeared to occur from the base. Type 2 growths had a similar layered structure, but grew to much greater heights (~1 mm) with a pronounced conical shape (Fig. 5). Type 3 growths (Fig. 6) were filamentary and less common, but when present tended to occur over large areas of the surface. The filaments were ~10 $\mu$m diameter and ~1 mm long and composed of equiaxed crystallites. Each filament was always associated with a surface pit (at A in Fig. 6) which extended from the base of the filament. All growth types grew rapidly, i.e. they were present after heating to 530° C in ~3 min and appeared similar on ground and electropolished surfaces. Because significant growth only occurred above 500° C, the minimum growth rates were 1.9 to 2.3 $\mu m\,sec^{-1}$. The dimensions of Types 1 to 3 growths did not appear to

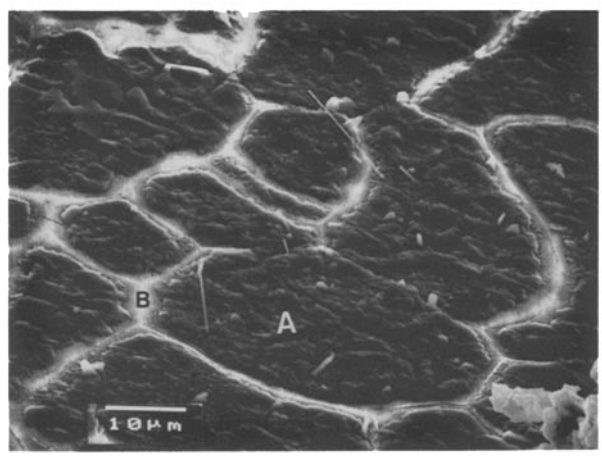


*Figure 2* Scanning electron micrograph (SEM) of unrecrystallized sheet, ground surface after 5 min at 530° C in air showing reduced oxidation at grain boundaries.

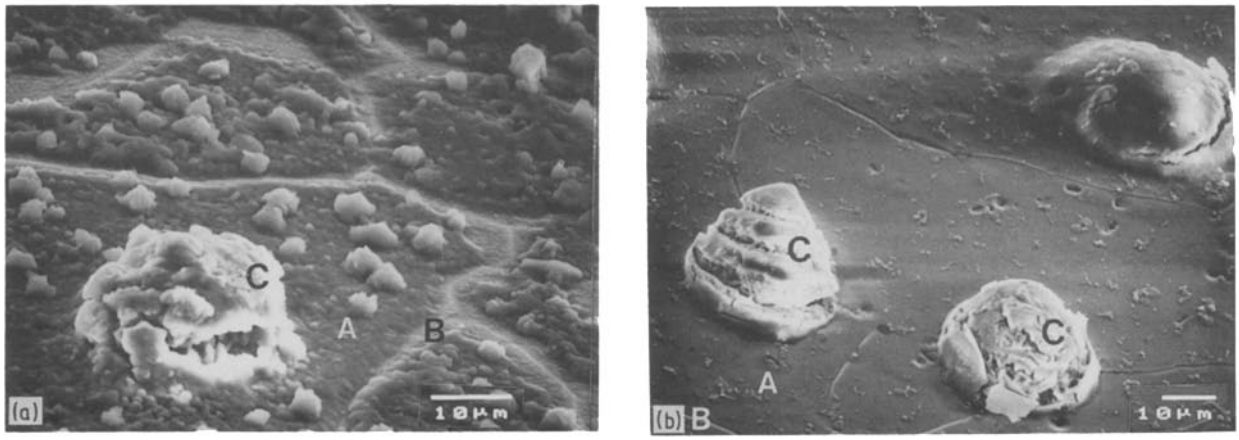


*Figure 3* SEM of recrystallized sheet after 1 min at 530° C: (a) ground surface in air; (b) electropolished surface in moist argon, showing Type 1 growths.

be sensitive to exposure times in the range 1 to 60 sec or to different moisture contents in air.

Type 4 growths consisted of small growth nodules at A surrounded by an oxidation-free halo with sometimes an outer thicker oxidation rim at B in Fig. 7. These sites were less obvious than Types 1 to 3 but were observed under many different oxidation conditions. The same area observed after reheating for 1 min at 530° C is shown in Fig. 7b; the central nodule remains at A but the oxidation-free halo at B has increased in area, i.e. the original film has disappeared. Fragmentation of the film during cooling seemed unlikely because the edge of the film at C was uncracked and no fragments were found on the surface. Both forms of Type 4 growth were equally common.

Type 1 growth appeared as black circular areas in optical micrographs and often occurred within grains as shown at A in Fig. 8a. A specimen surface was ground to 1 $\mu$m diamond surface finish in a direction normal to the rolling direction in the sheet. At low magnification Type 1 growths were clearly aligned parallel to the rolling direction (Fig. 8b) and not along the grinding direction as reported elsewhere [12].

### 3.3. Origin of rapid oxidation sites

A series of optical and scanning electron micrographs were obtained for the same area of surface before and after oxidation. The initial electropolished area of a recrystallized sheet with a scratch (S) for marker is shown in Fig. 9a; very small pits and insoluble particles are visible at positions marked 1, 2, 3, 4 and 5. After 1 min at 530° C in moist air the surface appeared as in Fig. 9b; the black areas corresponding to Type 1 growths are visible at the particle sites 1 to 5, together with a background film. After washing in water the background film was almost completely removed, but Type 1 growths remained. It was concluded that the growths were spinel. Ultrasonic cleaning for 2 min in water or acetone removed Type 1 growths and revealed large pits at the original positions of the growths 1 to 5 (Fig. 10a). The original electropolished pits visible in Fig. 9a were still visible in Fig. 10a and allowed precise location of the centres of the Type 1 pits in Fig. 10a. Each Type 1 pit coincided with a pre-existing particle, but not all particles visible had given rise to rapid oxidation.

The area in the optical micrograph in Fig. 9b is shown in a series of scanning electron micrographs in Figs 9d and e; note the surface is inclined in the SEM and the particle positions are changed slightly relative to the optical micrograph, but the scratch S is a reference point. In the oxidized state (Fig. 9c), nine Type 1 growths are visible and numbered 1 and 3 to 10. Those numbered 1, 3, 4 and 5 are the same as the corresponding numbered sites in Fig. 9b. Growths numbered 5 and 6 are shown at higher magnification in Figs 9d and e and are about 25 $\mu$m diameter at the base and about 25 $\mu$m long. After ultrasonic cleaning,

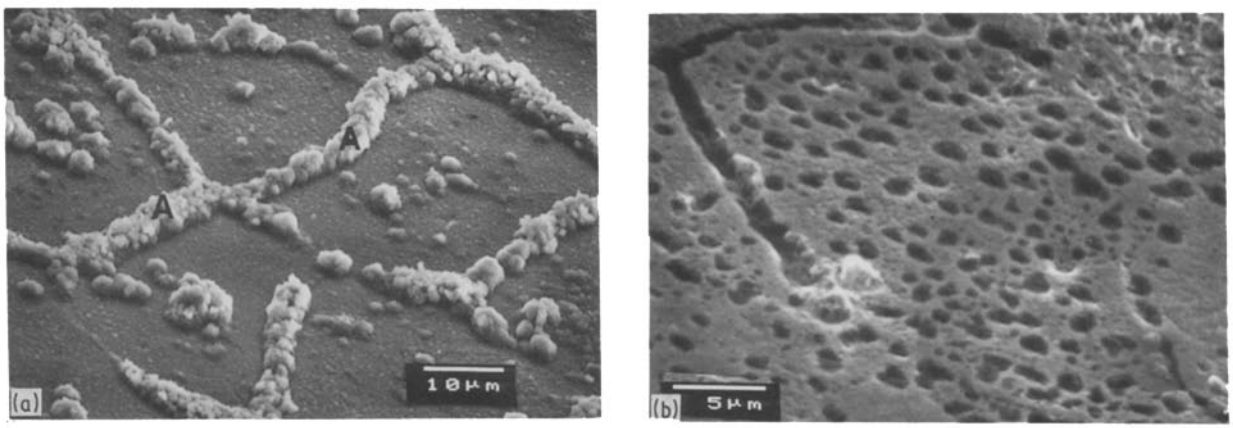


*Figure 4* SEM of recrystallized sheet, electropolished surface after (a) 2 min at 530° C in hydrogen, (b) after washing in water for 5 min.

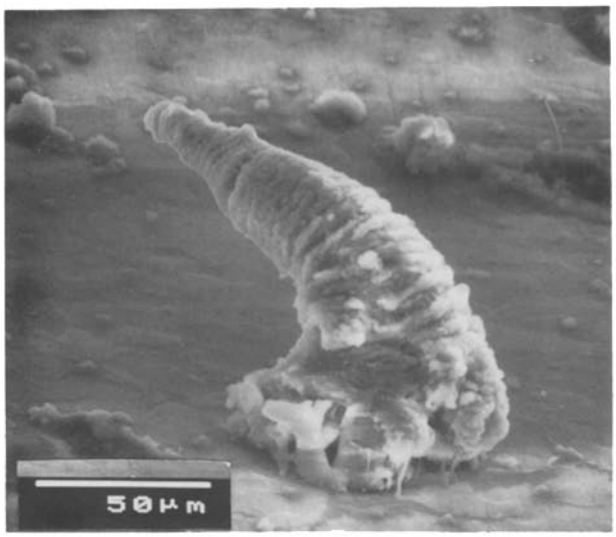


*Figure 5* SEM of unrecrystallized sheet, ground surface after 10 min at 530° C in air showing Type 2 growth.

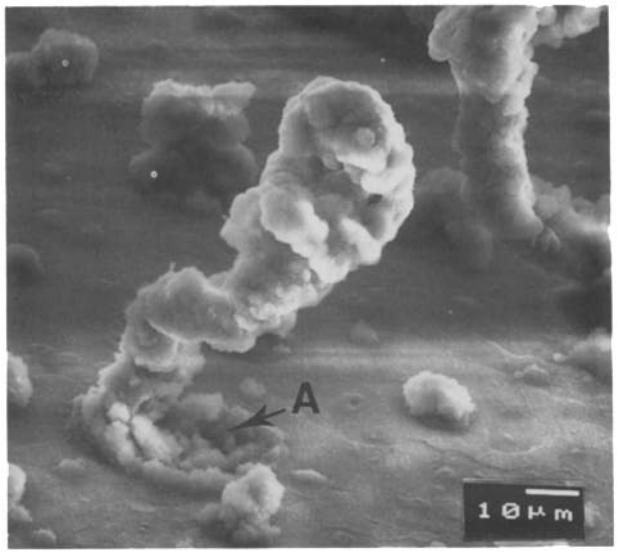


*Figure 6* SEM of unrecrystallized sheet, ground surface after 10 min at 530° C in air showing Type 3 growth.

the pits associated with growths 1 to 10 are shown in Fig. 10b; pits 5 and 6 are shown at higher magnification in Figs 10c and d. The growth diameter equalled the pit diameter. In the surface of the pits many holes were visible which led in different directions into the base metal. Note pit no. 6 in Fig. 10d lies within a grain. Pits were visible beneath all the rapid oxidation sites after ultrasonic cleaning. The pits were $\sim 25\,\mu m$ diameter and 10 to $20\,\mu m$ deep beneath Type 1 to 3 growths; this depth was several times the initial diameter of the grains in a direction normal to the sheet surface. At Type 4 growth sites the pits were $< 10\,\mu m$ diameter and very shallow.

### 3.4. Number and size of pits associated with rapid oxidation sites

All pits visible after ultrasonic cleaning beneath Type 1 and 2 growths tended to have circular cross-sections in the sheet plane. The number of pits and their diameters at the surface were measured on recrystallized and unrecrystallized sheet after 1 min and 1 h at 530° C in moist air. Three areas of $0.04\,mm^2$ were selected for each condition and the mean number of pits per unit area in each size range were measured.

The mean number of sites in the three areas and the total number of sites per $cm^2$ are given in Table III; the number of sites per $cm^2$ is plotted against pit diameter in Figs 11a and b. The variability in the number of sites per unit area over the surface and the small total area examined suggests the difference in numbers for the 1 min and 1 h exposure times in Figs 11a and b may not be significant, but the size distribution is believed to be valid. For both sheet conditions and for the two exposure times the pit diameters were in the range 5 to $35\,\mu m$ with the maximum number ($8.8 \times 10^3$ to $18.5 \times 10^3$ pits $cm^{-2}$) in the range 10 to $25\,\mu m$. The increase in exposure time by a factor 60 did not appear to increase dramatically either pit diameter (Figs 11a and b) or pit depth. The surface condition (1 $\mu m$ diamond polished or electropolished) did not appear to affect the results.

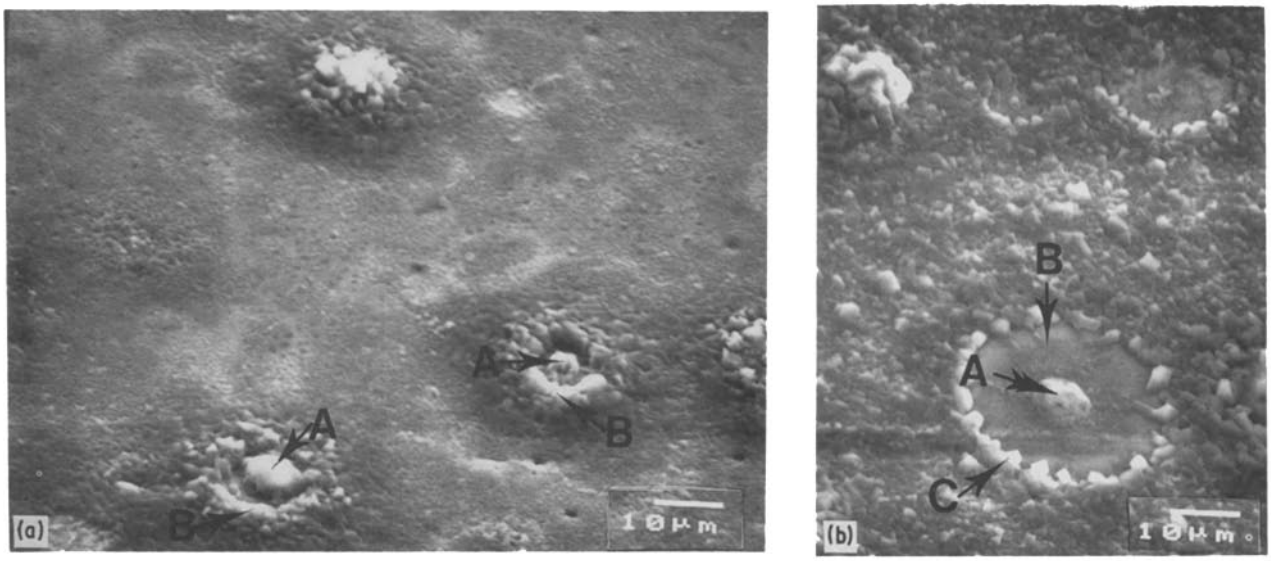


*Figure 7* SEM of recrystallized sheet, electropolished surface, (a) after heating to 500° C in moist air and removing immediately; (b) same area after reheating to 500° C for 1 min showing Type 4 growths.

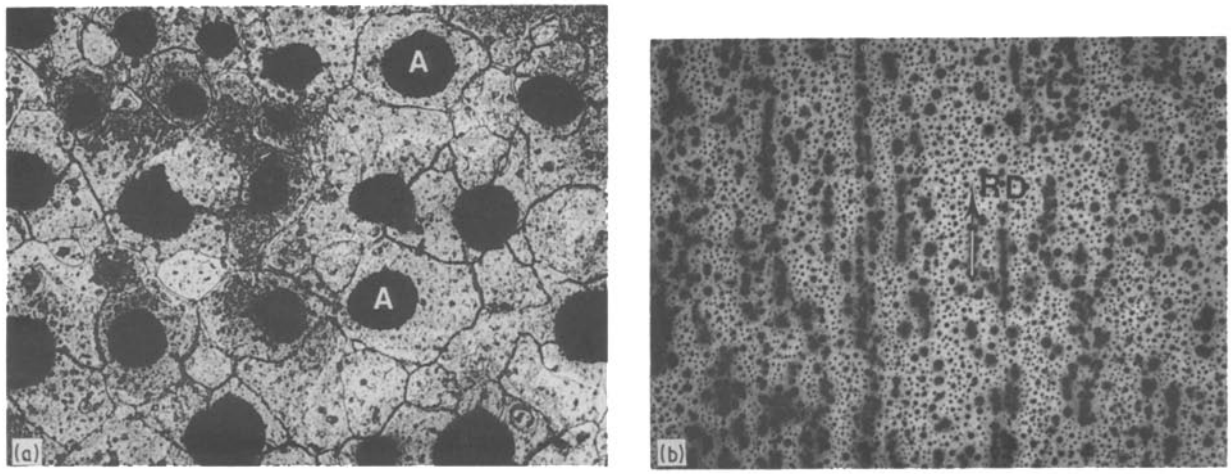


*Figure 8* Optical micrograph showing Type 1 growths after 1 min at 530° C: (a) recrystallized sheet, electropolished surface in moist argon, × 182; (b) unrecrystallized sheet ground surface in air, × 40.

## 4. Discussion

The difficulties encountered in studying the oxidation of Al–Li alloys have been summarized in Section 1. In the present programme it was not possible to identify directly the small volume fraction of oxidation product produced after short-time exposure. A tentative identification of the phases LiH, $LiAlO_2$ and $Li_2CO_3$ was, therefore, based upon the morphology and exposure conditions reported for these phases in the literature.

### 4.1. Grain-boundary oxidation

The reported preferential oxidation at grain boundaries during exposure in air [14] was not observed in the present work. In fact at short times, when the grain interior was covered with $Li_2CO_3$, the grain-boundary region appeared almost free of this oxidation product (Figs 2 and 3) and was analogous to the precipitate-free zone reported [9] for lithium-depleted grain boundaries near oxidized surfaces of 8090 alloy. The reduced grain-boundary oxidation in the present study is therefore attributed to the more rapid diffusion and loss of lithium from the grain-boundary region than from the grain interior during the heating up and exposure periods. The oxides that form subsequently at the grain boundaries will therefore be deficient in lithium, making the surface more resistant to oxidation. The time taken to form the dominant $Li_2CO_3$ phase will then be longer over these surfaces than over surfaces further from the grain boundary, as observed.

A similar explanation in terms of lithium depletion has been proposed for the occurrence of a plateau in the weight gain–time curves obtained after breakaway oxidation in Al–Li alloys [3].

TABLE III Number of rapid oxidation sites

| Sheet condition | Exposure time (min) | Mean number of sites per area of 0.04 mm² | Total number of sites per cm² $N$ ($10^{-3}$ cm$^{-2}$) |
|---|---|---|---|
| Recrystallized | 1 | 14 ± 1.4 | 38.9 |
| | 60 | 10.3 ± 2.9 | 28.0 |
| Unrecrystallized | 1 | 6.5 ± 0.6 | 16.4 |
| | 60 | 15 ± 1.4 | 38.3 |

The opposite effect was obtained in the hydrogen atmosphere when preferential oxidation formed thicker LiH films at the grain boundaries (Fig. 4a). A similar result was reported for Al–Li binary alloy exposed in hydrogen at 550° C for 2 h [13]. In both examples washing in water removed the LiH and revealed surface pits. Preferential grain-boundary oxidation in hydrogen is attributed to the absence of oxide films which allows the hydride film thickness to reflect the relative rates of diffusion along grain boundaries and in grain interiors.

### 4.2. A model for rapid local oxidation

Sites of rapid local oxidation have been reported in Al–Li and Al–Li–Mg alloys after $2\frac{1}{2}$ h in a moist $O_2$/Ar mixture at 480° C [3] and in 8090 alloy after 1 min in air at 530° C [12] but the origin of the sites was not known [2]. Although sites in 8090 were reported along the grinding grooves, this appears to be incorrect, because in the same alloy the present results clearly show the sites are associated with specific particles distributed in stringers aligned parallel to the rolling direction (Fig. 8b). This also explains the occurrence of rapid oxidation growths within the grain rather than at grain boundaries.

In some respects, particularly in an argon atmosphere, Type 1 growth in 8090 alloy resembles the growth of primary MgO crystals on Al–Mg alloy surfaces [18]. However, the sites on 8090 alloy were unique with respect to their size, growth rates, morphologies and association with particles. Because lithium diffusion is rate-controlling in the oxidation process [10, 12] the Type 1 to 3 growth behaviour suggests that the particles are providing a very effective pipe for lithium diffusion to a reaction zone. The qualitative model proposed for the rapid oxidation sites requires that the particles initiate or catalyse the reaction between lithium and oxygen and/or water vapour. The removal of lithium and aluminium to form the spinel growth creates a cavity which becomes a reaction zone or pit beneath the growths. As the pit increases in depth it penetrates several grains and many grain boundaries will intersect the surface of the pits. Diffusion via these grain boundaries will provide a high concentration of lithium for rapid growth of

the spinel. Local lithium concentration gradients that develop would tend to increase the pit depth at the expense of the diameter [19, 20]. Eventually the advancing surface lithium-depletion front will overtake the pit depth, grain growth will occur and the fast lithium supply will be cut off and rapid oxidation will cease. This model explains the transient nature of these rapid oxidation sites, including the cavities associated with Type 3 growths (Fig. 6), which are then a consequence of diffusion along grain boundaries parallel to the surface and towards the growth.

Some active particles in the present work were rich in copper or iron as found in Al–Li and Al–Li–Mg alloys [3] and in agreement with the particles of $Al_6CuLi$ and $Al_7CuFe$ suggested in the 8090 alloy [12]. However, it is not clear why so few particles were active.

The volume changes caused by the formation of the spinel can explain the penetration and cracking of surface films, but the suggestion that the hydrogen gas is responsible for these growth [3] does not seem consistent with their open microstructure. The disappearance of the surface film around Type 4 growths (Fig. 7) may be an example of the reaction $Li + Li_2CO_3 \rightarrow Li_2O + C$ [2], although no product film was visible.

### 4.3. Weight gain caused by rapid oxidation growths

It is possible to estimate the weight gain caused by Type 1 growths. Taking Type 1 growth pits to be hemispheres with depth $h$, diameter $2h$, and number

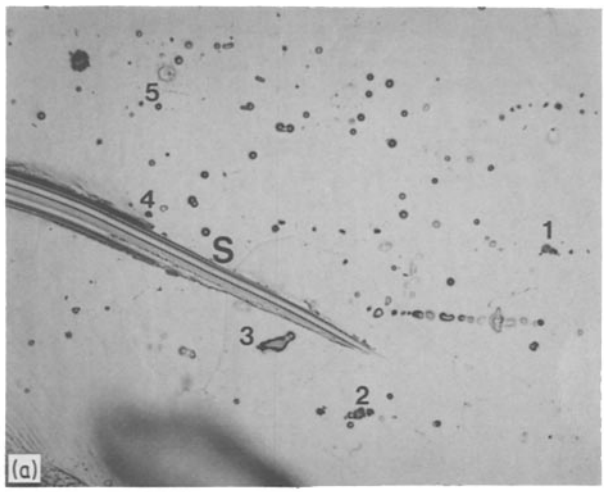


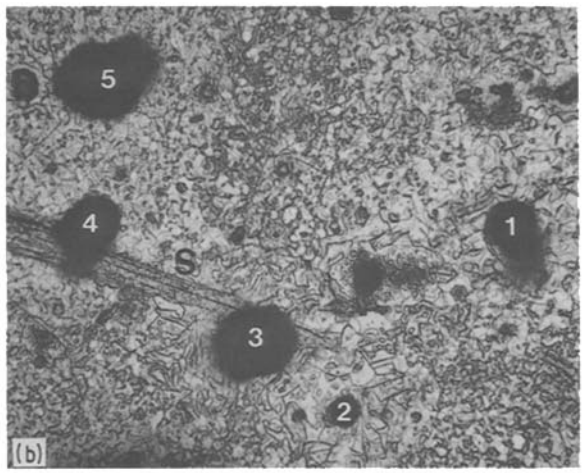


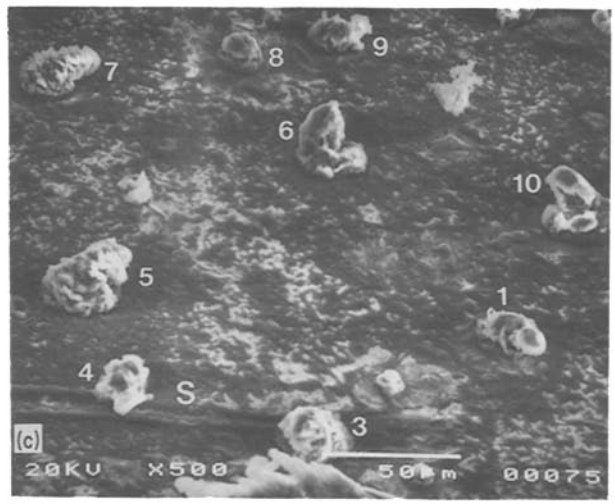


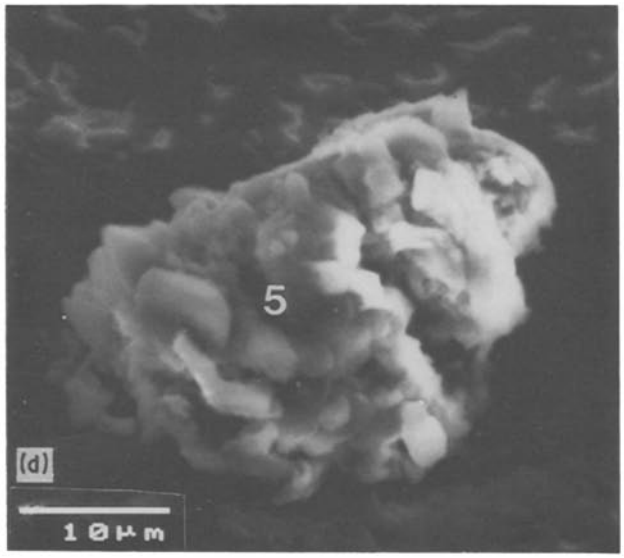


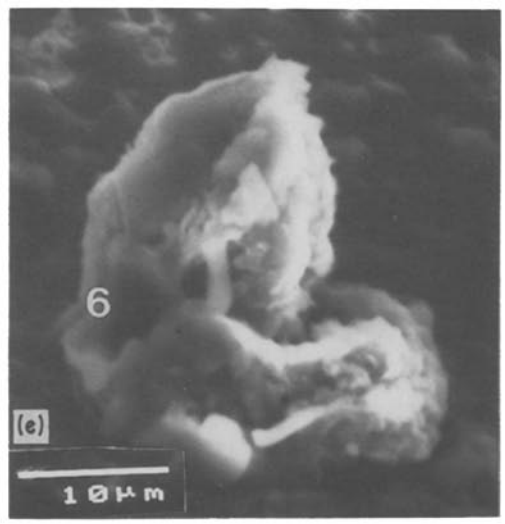


*Figure 9* Recrystallized sheet, optical micrographs of (a) electropolished surface with scratch marker at S × 376, (b) same area after 1 min at 530° C in moist air showing Type 1 growths numbered 1 to 5, and SEM covering the same area with scratch marker at S showing × 378 (c) Type 1 growths 1, 3 to 10, (d) Type 1 growth no. 5, and (e) Type 1 growth no. 6.

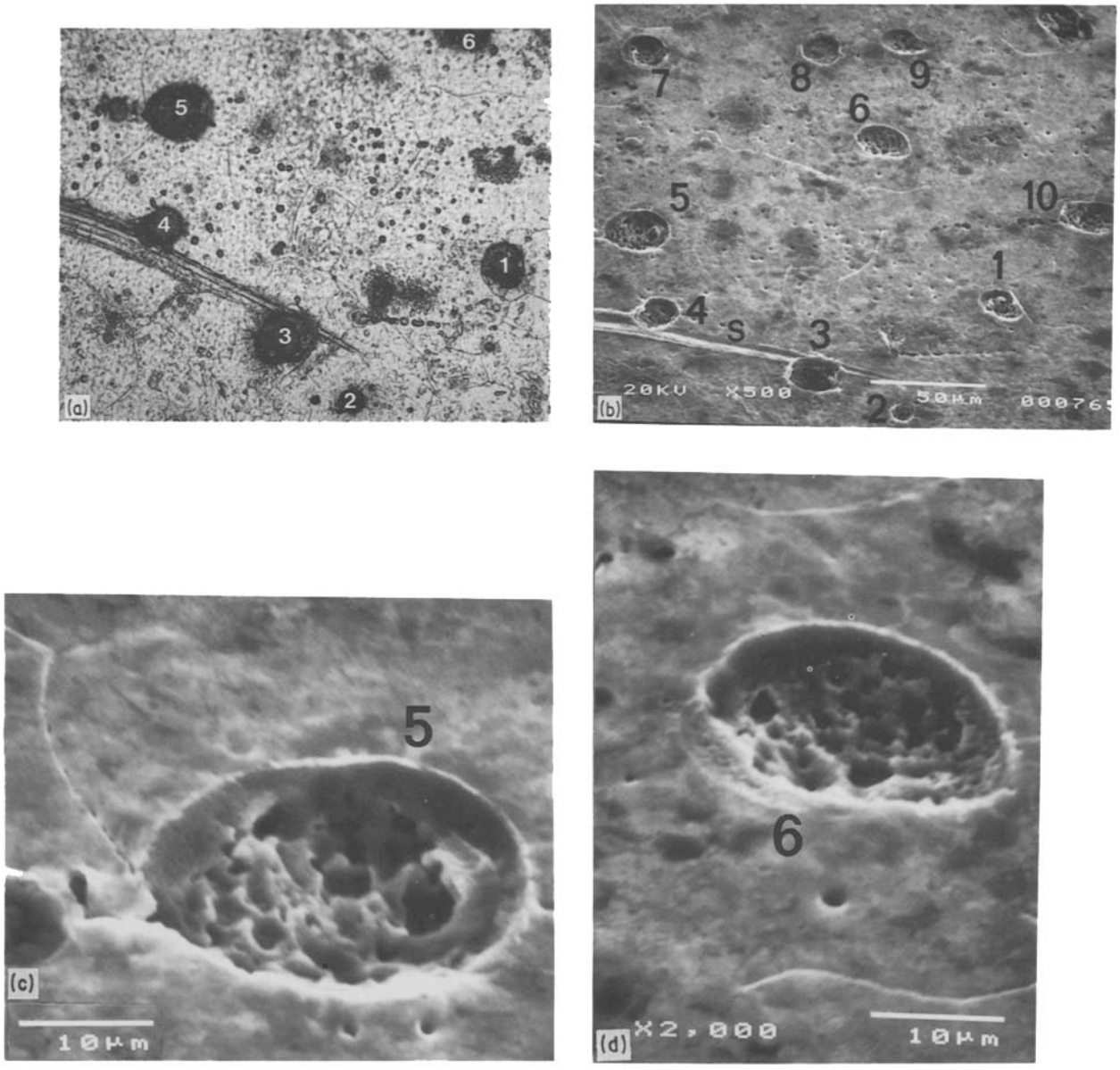


*Figure 10* Same area as in Fig. 9 after washing and ultrasonic cleaning in water, with scratch marker at S: (a) optical micrograph showing Type 1 pits numbered 1 to 6, ×352 and SEM (b) showing Type 1 pits numbered 1 to 10 and (c) Type 1 pit no. 5 and (d) Type 1 pit no. 6.

density $N\,\mathrm{cm}^{-2}$, then the total volume of all the pits is approximately

$$V = \tfrac{2}{3}\pi h^3 N\,\mathrm{cm}^{-2} \quad (5)$$

For the oxidation product $LiAlO_2$, the metal consumed to form the oxide would have the composition 50 at % Li, 50 at % Al with a density, $\varrho$, and weight $W_1 = V\varrho$. The oxide weight would be $W_2 = fV\varrho$ where $f$ is the ratio (oxide weight/metal weight). The weight gain is therefore

$$\Delta W = \tfrac{2}{3}\pi h^3 N\varrho(f - 1) \quad (6)$$

The calculated $\varrho$ for 50 at % Li, 50 at % Al is $\sim 1.5\,\mathrm{g\,cm}^{-3}$, and $f = 1.94$ (Table II), $N \sim 3 \times 10^4\,\mathrm{cm}^{-2}$ (Figs 11a and b), and $h \sim 10\,\mu\mathrm{m}$ which, from Equation 6, gives $\Delta W \approx 0.1\,\mathrm{mg\,cm}^{-2}$. This is the weight gain due to oxidation by Type 1 growth alone in a time 1 to 5 min for a conservative pit depth of 10 $\mu$m.

The estimated weight gain is very close to the reported values for 8090 alloy [10, 11]. Bearing in mind the steep slope to the weight gain curves at times $< 5$ min and the onset of continuous $Li_2CO_3$ film formation only after times $> 5$ min, the results suggest that rapid oxidation growths may account for all the weight gains in the initial stages of oxidation.

### 4.4. Effect of rapid oxidation sites on mechanical properties

The recommended solution heat-treatment time for 1.6 mm 8090 sheet is 5 to 30 min [15, 16]. For multiple heat treatments in the presence of moisture, lithium loss and pits associated with rapid oxidation may have a detrimental effect on the properties of thin sheet. Lithium surface depletion is known to decrease the tensile strength [9, 15, 16] but the effect on fatigue is less clear [9]. The mechanical removal of the depleted layer would probably remove the pits produced by oxidation. However, etching of oxidized surfaces produced surface pitting with a maximum pit size of 200 $\mu$m diameter and 30 $\mu$m depth [1]. This pitting may be caused by pre-existing oxidation pits. The oxidation

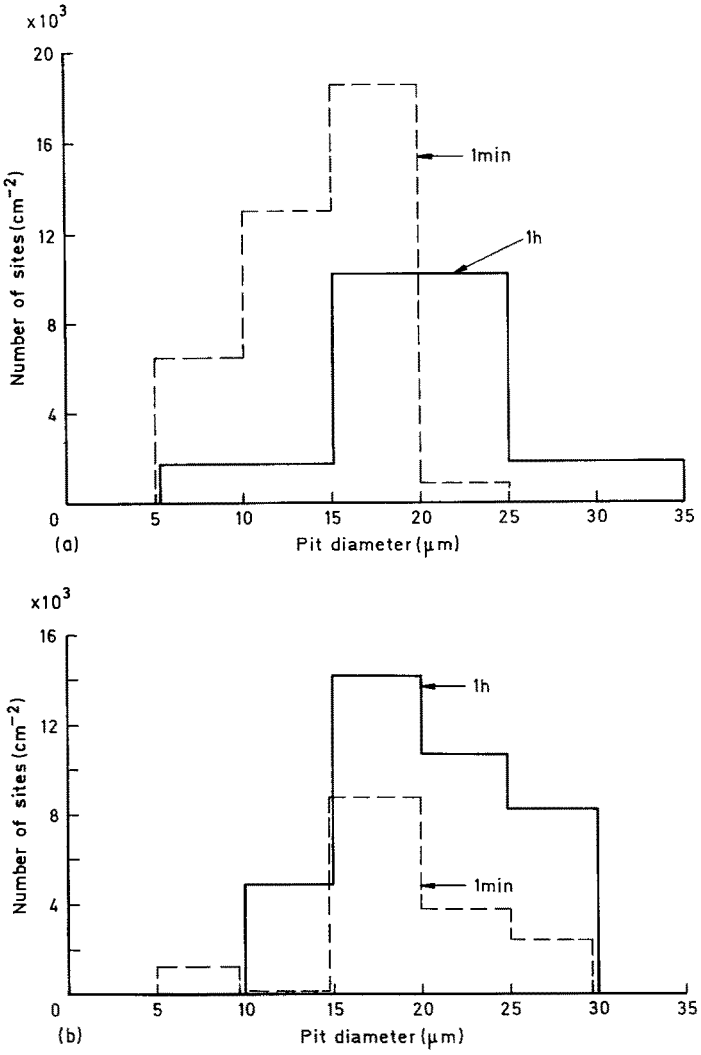


*Figure 11* Type I pit diameter distribution and number density for (a) recrystallized and (b) unrecrystallized sheet after exposure at 530° C in moist air for 1 min and 1 h followed by washing and ultrasonic cleaning.

pit depth is comparable with that reported for pits on pickled 8090 alloy sheet [9] and these led to reduced fatigue life. Thus pits associated with rapid oxidation sites may adversely affect the fatigue life, but their effect will depend on the surface-cleaning processes used and on section thickness.

The results also suggest that in the presence of moisture or oxygen, oxide-filled pits will occur rapidly on 8090 alloy surfaces at temperatures of 530° C and above, the temperature range used for diffusion bonding. These pits will decrease the bond strength. When the concentration of the above gases is kept very low, however, parent metal bond strengths can be obtained in 8090 alloy sheet [21].

## 5. Conclusions

1. Semi-continuous thin films and sites of rapid local oxidation occurred on 8090 alloy sheet oxidized in laboratory air or moist atmospheres for short times at 530° C.

2. Preferential grain-boundary oxidation occurred in hydrogen but not in laboratory air or moist argon. This was attributed to the resistance to oxidation by lithium-depleted oxide films at the grain boundaries in air or moisture. In hydrogen the film reflected the different rates of lithium diffusion.

3. Sites of rapid local oxidation occurred at insoluble particles. Their number density was 9 to 18 $\times$ $10^3$ $cm^{-3}$ and some growths, believed to be spinel, were 10 to 25 $\mu$m diameter and grew to $\sim$ 1 mm in height at a rate greater than $\sim 2\,\mu m\,sec^{-1}$. Pits 25 $\mu$m diameter and 10 to 20 $\mu$m deep developed below some growths.

4. A qualitative model to explain the oxide growth characteristics at these sites is based upon rapid lithium diffusion along the grain boundaries.

5. The pits associated with oxidation sites may reduce the fatigue strength depending on the surface treatments and section thickness; the formation of these oxide-filled pits may reduce the strength of diffusion-bonded joints.

6. Spinel growth at these sites can account for all the weight gain during short-time oxidation.

## Acknowledgements

The authors are grateful for the support provided by D. V. Dunford and Jane M. Gorringe in the experimental work. This work is published by permission of the Controller, H.M.S.O., holder of Crown Copyright.

## References

1. M. BURKE and J. M. PAPAZIAN, "Aluminium alloys III" (Institute of Metals, London, 1986) p. 287.
2. K. WEFERS and F. A. MOZELEWSKI, Proceedings 8th International Light Metals Conference, Vienna (1987) p. 744.
3. D. J. FIELD, E. P. BUTLER and G. M. SCAMANS, Proceedings 1st International Al–Li Conference (Metals Society, AIMME, Warrendale, Pennsylvania, 1981) p. 325.
4. D. J. FIELD, G. M. SCAMANS and E. P. BUTLER,

Proceedings 2nd International Al–Li Conference (Metals Society, AIMME, Warrendale, Pennsylvania, 1984) p. 657.
5. I. N. FRIDLYANDER, V. S. SANDLER, T. I. NIKD' SKYA, R. A. SAVINKOV and I. N. ROSCHINA, *Russ. Met.* **2** (1978) 175.
6. A. CSANADY and J. KURTHY, *J. Mater. Sci.* **16** (1981) 2919.
7. A. CSANADY, D. MARTON, I. GELEJI-NEUBAUER, S. HOFMANN and J. M. SANZ, *Corrosion Sci.* **22** (1982) 689.
8. A. CSANADY, T. TURMEZEY, I. IMRE-BAAN, A. GRIGER, D. MARTON, L. FORDOR and L. VITALIS, *ibid.* **24** (1984) 237.
9. S. FOX, H. M. FLOWER and D. S. McDARMAID, Proceedings 3rd International Al–Li Conference (Institute of Metals, London, 1986) p. 263.
10. J. M. PAPAZIAN, R. L. SCHULTE and P. N. ADLER, *Met. Trans.* **17A** (1986) 635.
11. J. M. PAPAZIAN, J. P. W. WAGNER and W. D. ROONEY, 4th International Al–Li Conference, Paris *J. Physique* **48** (1987) p. C3–513.
12. M. AHMAD, *Met. Trans.* **18A** (1987) 681.
13. R. C. DICKINSON, K. R. LAWLESS and E. WEFERS, *Scripta Metall.* **22** (1988) 917.
14. R. F. ASHTON, D. S. THOMPSON, E. A. STARKE and F. S. LIN, International Al–Li Conference III (Oxford Inst. Metals, 1986) p. 66.
15. J. M. PAPAZIAN, G. G. BOTT and P. SHAW, 17th National SAMPE Technical Conference (1985) p. 688.
16. *Idem, Mater. Sci. Engng* **94** (1987) 219.
17. D. CONSTANT, M. DOUDEAU and P. MEYER, AGARD Al–Li Conference, Mierlo to be published.
18. D. J. FIELD, G. M. SCAMANS and E. P. BUTLER, *Met. Trans.* **18A** (1987) 463.
19. C. WAGNER, *Electrochem. Soc.* **103** (1956) 571.
20. H. W. PICKERING and Y. S. KIM, *Corrosion Sci.* **22** (1982) 621.
21. D. V. DUNFORD and P. G. PARTRIDGE, to be published.

*Received 27 October*
*and accepted 10 November 1988*